

^3He flow in dilute ^3He - ^4He mixtures at temperatures between 10 and 150 mK

C. A. M. Castelijns, J. G. M. Kuerten, A. T. A. M. de Waele, and H. M. Gijssman
Eindhoven University of Technology, Eindhoven, The Netherlands

(Received 12 December 1984)

The mutual friction between ^3He and ^4He II below 150 mK has been studied. Empirical relations for the adiabatic and the nonadiabatic flow properties of ^3He moving through ^4He have been determined using a dilution refrigerator with a single mixing chamber. The validity of the relations is verified by osmotic-pressure measurements and by measuring the properties of a double-mixing-chamber system. It is shown that superleak shunts have a strong effect on the flow characteristics. From the nonadiabatic flow properties an expression is derived for the mutual-friction-force density between ^3He and ^4He II. This has a strong resemblance to the Gorter-Mellink mutual-friction-force density between the normal and the superfluid components in pure ^4He II. It is speculated that the ^3He flow in our systems generates a ^4He vortex tangle, which leads to the observed mutual friction between ^3He and ^4He and also to a strong clamping of the ^4He to the walls.

I. INTRODUCTION

In the hydrodynamics of ^3He - ^4He mixtures, the mutual friction between ^3He and ^4He plays an important role.¹ As a consequence, the hydrodynamic equations, based on the model in which the mutual friction is neglected^{2,3} [the mechanical-vacuum (MV) model], cannot be in agreement with the experimentally observed behavior. In our laboratory new empirical relations for the adiabatic flow properties have been determined.⁴

In this paper we report on further results of our experiments concerning the variations of liquid properties as functions of the ^3He flow rate and the tube dimensions. In general, flow channels of cylindrical shape (tubes), of which the length is an order of magnitude larger than the diameter, will be considered. Attention will be paid to pressure, osmotic-pressure, temperature, and ^3He -concentration measurements in the steady state, using a single mixing chamber. Furthermore, the influences of superleak shunts across the tubes on the flow properties will be discussed. A new description of the operation of a double mixing chamber⁵ will be given, based on the empirical relations derived from our experiments.

Section II deals with the flow properties determined with a single mixing chamber. In Sec. III the double mixing chamber will be considered. In both cases we will give a short discussion of the consequences of the MV model for the system, a description of the experimental setup, and the experimental results. In Sec. IV an expression for the mutual-friction-force density will be derived, our results will be compared with the results obtained by others, and we will speculate on the physical phenomena behind the observations.

II. SINGLE MIXING CHAMBER

A. Mechanical-vacuum model

1. Enthalpy balance

The law of conservation of energy for a steady flow of ^3He through ^4He II in a restricted geometry (flow resistance) reads

$$\dot{n}_3\mu_3 + \dot{n}_3TS_F + \dot{Q} = \text{const} , \quad (1)$$

in which \dot{n}_3 is the ^3He molar flow rate, \dot{Q} is the heat flow rate, T is the temperature, μ_3 is the ^3He molar chemical potential, and S_F is the entropy of the mixture per mole ^3He . The molar flow rate \dot{n}_4 of the ^4He component is assumed to be zero. Equation (1) can be written in the form of an enthalpy conservation law in which the enthalpy H_3^* is given by

$$H_3^* = \mu_3 + TS_F . \quad (2)$$

A treatment of the thermodynamic quantities of liquid ^3He - ^4He mixtures is given by Kuerten *et al.*⁶ The limiting values for ^3He concentrations near saturation and temperatures near absolute zero, are summarized in the Appendix.

Using Eqs. (1) and (2), the variation of the thermodynamic properties in a cylindrical tube with length L and diameter D can be calculated in the same way as did Wheatley *et al.*³ and van Haeringen,⁷ starting from the Gibbs-Duhem relation for ^3He - ^4He mixtures

$$x d\mu_3 + (1-x)d\mu_4 = -S_m dT + V_m dp , \quad (3)$$

in which μ_4 is the molar chemical potential of the ^4He component, x is the ^3He molar concentration, p is the pressure, and S_m and V_m are the entropy and volume per mole mixture. At very low temperatures the contribution of the ^4He component to the total entropy of the mixture can be neglected. Hence,

$$S_m = xS_F . \quad (4)$$

In the MV model the mutual friction force between ^3He and ^4He is assumed to be zero. In that case, in the steady state, μ_4 is constant:

$$\mu_4 = \text{const} . \quad (5)$$

Combining Eqs. (1)–(5) leads to

$$\dot{n}_3 T dS_F + \dot{n}_3 V_3 dp + d\dot{Q} = 0 , \quad (6)$$

where $V_3 = V_m/x$ is the volume per mole ³He. The heat flow \dot{Q} is given by

$$\dot{Q} = -\frac{\pi D^2}{4} \kappa \frac{dT}{dl} \quad (7)$$

In Eq. (7) l is the distance from the tube entrance and κ the coefficient of thermal conductivity.

Within the framework of the MV model, the ³He is assumed to flow with a certain viscosity η equal to the viscosity of the total mixture as measured by Kuenhold *et al.*⁸ The pressure change, assuming Poiseuille flow, is given by

$$dp = -\eta \dot{n}_3 V_3 \frac{128}{\pi D^4} dl \quad (8)$$

Hydrostatic-pressure changes will not usually be considered in this paper. However, in a few important cases, when the pressure variations due to the ³He flow are on the order of 1 Pa, they may play a dominant role. The radial distribution of the molar-flow-rate density j_3 is given by

$$j_3 = \frac{8\dot{n}_3}{\pi D^4} (D^2 - 4r^2), \quad (9)$$

where r is the distance from the tube axis.

At very low temperatures S_F , κ , and η can be approximated by their low-temperature values (see the Appendix). Substitution of these approximations in Eqs. (6), (7), and (8) leads to a differential equation for the T - l relationship, which can be written in dimensionless form by introducing the dimensionless parameters τ and λ according to

$$\lambda = l/L_0 \quad (10)$$

and

$$\tau = T/T_0, \quad (11)$$

in which L_0 and T_0 are given by

$$L_0 = \frac{\pi}{2} \left[\frac{\kappa_0^2}{128 C_0 \eta_0 V_3^2} \right]^{1/3} \frac{D^{8/3}}{\dot{n}_3} \quad (12)$$

and

$$T_0 = \left[\frac{128 \eta_0 V_3^2 \kappa_0}{C_0^2} \right]^{1/6} D^{-1/3}. \quad (13)$$

The differential equation for the T - l relationship can then be transformed to

$$\frac{d\tau^2}{d\lambda} - \frac{1}{\tau^2} - \frac{d}{d\tau} \left[\frac{1}{\tau} \frac{d\tau}{d\lambda} \right] = 0. \quad (14)$$

2. The p , T , x , and Π profiles in tubes

Equation (14) and the scaling parameters T_0 and L_0 play a central role⁹ in dilution refrigeration; e.g., it can be shown that dilution refrigerators should have an intrinsic low-temperature limit equal to $0.7T_0$.³ The solutions of Eq. (14) are described by van Haeringen.⁷ His analysis shows that in the main part of long tubes (length $L \gg L_0$) at higher temperatures ($T > T_0$), the thermal-conductivity

term can be neglected. In that case, Eq. (14) reduces to

$$\frac{d\tau^2}{d\lambda} - \frac{1}{\tau^2} = 0. \quad (15)$$

Integration gives

$$T^4 = T_m^4 \left[1 + \frac{128l}{\pi D^4} \frac{4V_3^2 \eta_0}{C_0 T_m^4} \dot{n}_3 \right], \quad (16)$$

where T_m is the temperature at the tube entrance. In our experiments the entrance is usually situated in the dilute phase in the mixing chamber of a dilution refrigerator. If the heat flow \dot{Q} can be neglected, integration of Eq. (6) gives

$$p = p_m - \frac{C_0}{2V_3} (T^2 - T_m^2). \quad (17)$$

At low temperatures the fountain pressure can be neglected. In that case, it follows from Eq. (5) that

$$p - \Pi = \text{const}. \quad (18)$$

From the low-temperature limit of Π (see the Appendix) and from Eqs. (17) and (18),

$$T^2 = T_m^2 - b(x - x_m), \quad (19)$$

where b is given in the Appendix [Eq. (A9)]. Combining Eq. (16) with (19) gives an expression for the concentration profile in the tube:

$$x = x_m - \frac{T_m^2}{b} \left[\left(1 + \frac{128l}{\pi D^4} \frac{4V_3^2 \eta_0}{C_0 T_m^4} \dot{n}_3 \right)^{1/2} - 1 \right]. \quad (20)$$

The relations (9), (16), (17), and (20) form a complete set of equations from which the j_3 , T , p , and x profiles in the tube can be calculated from \dot{n}_3 , T_m , and the tube dimensions. They result from the basic assumptions of the MV model as expressed in Eqs. (5), (8), and (9).

3. Superleak shunts

A superleak S usually consists of a tube filled with fine powder. Viscous fluids like ³He cannot flow through the pores of the powder, but superfluid ⁴He can pass without dissipation. The ⁴He chemical potential μ_4 is constant over such a superleak.

The validity of the MV model can be tested in a direct way by comparing the measured flow properties in a tube Z shunted by a superleak S , with the properties of Z alone. This can be understood as follows.

The net ³He flow rate through Z is always equal to the externally applied ³He flow rate \dot{n}_3 , whether Z is shunted by a superleak or not. On the other hand, the ⁴He flow rate in Z may be modified significantly by inserting S : without S the net ⁴He flow in Z is zero. However, with $S||Z$, the ⁴He component may circulate internally through the tube and back through the superleak. Therefore, the relative motion of the two components in Z may be significantly different in the two cases. In the MV model the effects of the relative motion of the two components are assumed to be negligible. Hence, the system

properties should be independent of the motion of the ^4He . In other words, if μ_4 were constant in the tube even without the superleak shunt, then the p , T , x profiles for given \dot{n}_3 , measured before and after the installation of a superleak, should be the same.

In the first dilution refrigerator, built by Das, de Bruyn Ouboter, and Taconis¹⁰ in 1964, the dilute-flow channel was shunted by a superleak. Unfortunately, the effects of the superleak on the ^3He - ^4He flow properties had not been analyzed in more detail at that time.

B. Experimental setup

1. Dilution refrigerator

In Fig. 1 a schematic drawing is given of the low-temperature parts of a ^3He -circulating dilution refrigerator with a single mixing chamber. The machine used in our experiments has been described in more detail elsewhere.¹¹ The total circulation rate \dot{n}_t , measured with a

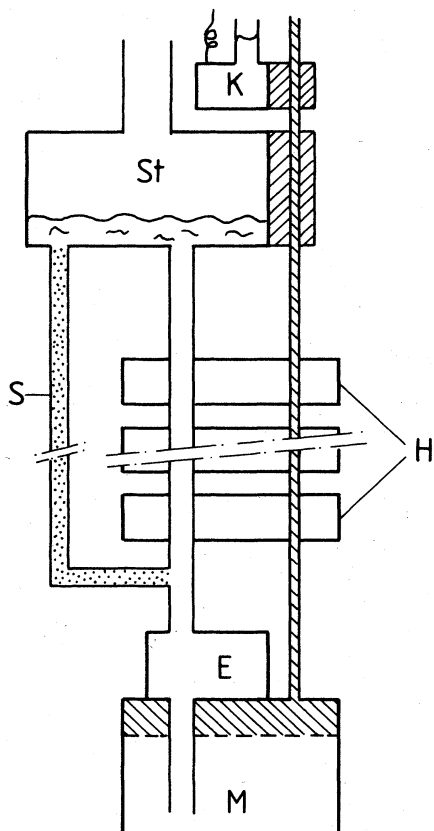


FIG. 1. Schematic drawing of the low-temperature part of the dilution refrigerator used in our experiments. *M*: Mixing chamber; *E*: experimental space; *H*: heat exchangers; *St*: still; *K*: 1-K plate; *S*: superleak (optional).

flow meter at room temperature, is the sum of the ^3He and ^4He circulation rates:

$$\dot{n}_t = \dot{n}_3 + \dot{n}_4. \quad (21)$$

The circulation rate \dot{n}_t could be varied between 0.13 and 2.5 mmol/s by varying the heating power \dot{Q}_s to the still. The ^4He flow rate \dot{n}_4 was typically 3% of \dot{n}_t (see Sec. C 1).

In our experiments heat leaks were negligible. The minimum temperature was limited by the heat-exchanger performance. With a single mixing chamber in the continuous mode it was about 10 mK.

2. Mixing-chamber and experimental space

Schematic drawings of the measuring system are given in Figs. 1 and 2. The mixing-chamber part *M* was made of stainless steel (inner diameter 38 mm, height 78 mm).

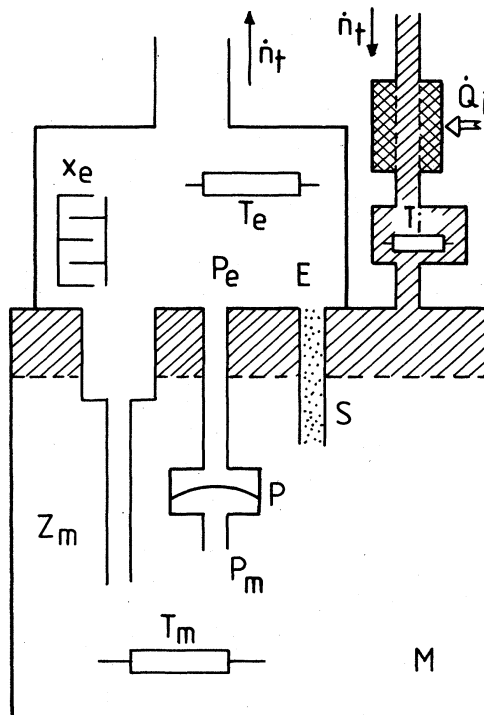


FIG. 2. Schematic drawing of the mixing chamber *M* and experimental space *E*. Between *M* and *E*, a flow resistance Z_m , a superleak *S*, and a differential pressure gauge *P* could be installed. Temperatures T_i , T_m , and T_e were usually measured by calibrated Speer carbon resistors. The ^3He concentration x_e in *E* was measured with an air capacitor. Temperature T_i could be varied with a heater \dot{Q}_i at the entrance tube.

An experimental space E (inner diameter 30 mm, height 34 mm) was part of the top of the mixing chamber. The ${}^3\text{He}$ entered E at the bottom. The other side of E was connected to the dilute side of the heat exchangers through a tube with inner diameter 5 mm and length 250 mm.

In general, the flow impedances studied were cylindrical tubes with $L \gg D$. The lengths varied from 5 mm to 1.4 m; the diameters from 0.3 to 2.3 mm. The tube under investigation, Z_m , was mounted between M and E . Furthermore, a superleak and a pressure cell could be installed between M and E , parallel to Z_m . During certain experiments (e.g., the calibration of the thermometers in E), Z_m consisted of a short tube with a relatively large diameter. This situation will be referred to as $Z_m = 0$.

In the nonadiabatic flow experiments a heating power \dot{Q}_z was supplied by a heater consisting of a copper body with a copper-powder sinter sponge (surface area 1 m^2) in order to keep the temperature of the heater body low. Twelve parallel channels (inner diameter 2 mm, length 23 mm) provided a passage for the flowing ${}^3\text{He}$ with practically zero flow resistance.

The temperature T_e in E was usually substantially higher than T_m . Therefore, in principle, heat flowed from E to M . However, the thermal contact between the liquids in E and M was negligible due to the high Kapitza resistances and the poor thermal conductivity of the liquid in Z_m . The heat flow to E via the connecting tube to the heat exchangers was also negligible.

The temperature T_i of the ${}^3\text{He}$ flowing into the mixing chamber could be varied by supplying a heating power \dot{Q}_i . The surface area of this sinter sponge was 0.5 m^2 . Using this heater, T_m could be varied independently of the other variables, such as \dot{Q}_s or \dot{Q}_z , within certain limits.

For $T_i > 500 \text{ mK}$, boiling of the liquid in the inlet tube occurred. In that case the dilution refrigerator failed to operate properly. Therefore, T_i was limited to values below 500 mK and, as a consequence, $T_m < 150 \text{ mK}$.

3. Thermometry

A superconductive fixed-point device, a cerium magnesium nitrate (CMN) thermometer, and resistance thermometers were used for the temperature measurements. All thermometers were placed in the liquid. The superconductive fixed-point device SRM 768 is described by Schooley *et al.*¹² External magnetic fields were screened by a metal cylinder with a high magnetic permeability (μ -metal). The superconducting transitions were detected with an ac current of $10 \mu\text{A}$ rms and a frequency of 329 Hz through the primary coil. The CMN thermometer was calibrated against the superconductive fixed-point device. The resistance thermometers in the low-temperature part of the dilution refrigerator were of the Speer type. They were calibrated against the fixed-point device and the CMN thermometer. The thermometers in the experimental space E were calibrated while $Z_m = 0$, in which case, $T_e = T_m$.

4. ${}^3\text{He}$ concentrations

The ${}^3\text{He}$ concentration x_e of the liquid in E was determined with an air capacitor, using the property that the

dielectric constant ϵ_r of a ${}^3\text{He}$ - ${}^4\text{He}$ mixture is a linear function of x (Ref. 13) according to

$$\epsilon_r = 1.0572 - 0.0166x. \quad (22)$$

The capacitor had a nominal value of 32 pF and a plate distance of 0.2 mm. It was calibrated by measuring the capacitance in vacuum, in pure ${}^4\text{He}$, and in a 6.6% mixture, respectively. The latter value was obtained in experiments with $Z_m = 0$ or from the extrapolation of the $x_e - \dot{n}_t$ dependence (see Fig. 6) to zero flow rate.

5. Osmotic pressure

The osmotic pressures Π_e and Π_m of the mixtures in E and M , respectively, were obtained from the measured temperatures and concentrations.⁶ The osmotic pressure Π_s in the still was measured with a so-called London device.¹⁴ With this technique the value of the osmotic pressure is derived from the temperature at which the osmotic pressure is balanced by the fountain pressure. This temperature was about 1.3 K. The resistance thermometer (Allen-Bradley, 56 Ω ; $\frac{1}{2}$ W) in the London device was calibrated against the vapor pressure of ${}^4\text{He}$ with an accuracy of 25 mK. Due to the strong temperature dependence of the fountain pressure, this led to an accuracy in Π_s of a few times 100 Pa; the resolution was on the order of 10 Pa. The uncertainty of the calibration was removed to some extent by shifting the calibration curve slightly in such a way that the measured fountain pressure was equal to Π_e at low flow rates.

6. Pressure changes

The pressure gauge consisted of two spaces (connected to M and E , respectively, see Fig. 2) separated by a Kapton foil (thickness $25 \mu\text{m}$). A silver layer was evaporated onto the foil and another onto a surface of the gauge body. The capacitive coupling between the two silver layers was on the order of 2.5 pF and is a function of the pressure difference across the foil. The gauge was calibrated in a ${}^4\text{He}$ cryostat against the hydrostatic pressure of a ${}^4\text{He}$ -liquid column. The sensitivity was 480 ± 30 aF/Pa. The resolution was 0.2 Pa.

7. Experimental procedure

Modifications in the system, such as changing tubes, inserting or removing superleaks, etc., were made at room temperature. After closing the cryostat, the first data could be taken after 24 hours. When a parameter, such as \dot{Q}_s , \dot{Q}_i , or \dot{Q}_z was changed, a new steady state was reached after one hour. In this paper only steady-state properties will be reported. In a usual sequence of measurements, one parameter (such as T_m) was fixed, while another (such as \dot{Q}_s or \dot{Q}_z) was varied.

With a heater, the superleak S , shunted parallel to the heat exchangers (Fig. 1), could be warmed locally above the λ point during a run. Thus, the system could be studied with and without a superleak shunt across the heat exchangers while the system remained at low temperatures.

C. Experimental results

1. Flow rates

The relation between the total circulation rate \dot{n}_t and the heating power to the still \dot{Q}_s is dependent on the flow resistance of the dilute channel and on the presence of superleaks in the system. First we will discuss the situation in which the flow resistance Z_m in the mixing chamber is negligible ($Z_m=0$). The results are plotted in Fig. 3. The squares represent the \dot{n}_t - \dot{Q}_s dependence, measured when the heat exchangers were *not* shunted by the superleak S shown in Fig. 1. At $\dot{n}_t=0.92$ mmol/s, the curve shows a kink.¹⁵ For circulation rates below the kink, $d\dot{Q}_s/d\dot{n}_t=33$ J/mol; in the other part of the curve, $d\dot{Q}_s/d\dot{n}_t=74$ J/mol.

The appearance of the kink can be explained as follows: at low flow rates an increase of \dot{Q}_s leads mainly to an increase of \dot{n}_3 and not of \dot{n}_4 . The slope of the \dot{Q}_s - \dot{n}_t curve then corresponds to the latent heat of evaporation of ^3He . At high flow rates, increasing \dot{Q}_s mainly increases \dot{n}_4 ; the slope corresponds to the latent heat of evaporation of ^4He . Apparently, at circulation rates corresponding to the kink or higher, the ^3He concentration in the liquid in the still is very low, due to a flow resistance somewhere in the dilute channel.

In Fig. 3 the \dot{n}_t - \dot{Q}_s dependence is also given as measured with a superleak connection between the still and the dilute exit tube of the mixing chamber ($S||H$). The kink in the \dot{n}_t - \dot{Q}_s curve has disappeared due to a reduction of the effective flow resistance of the dilute channel by the superleak shunt.^{1,15}

In order to extend the ^3He flow-rate region of our

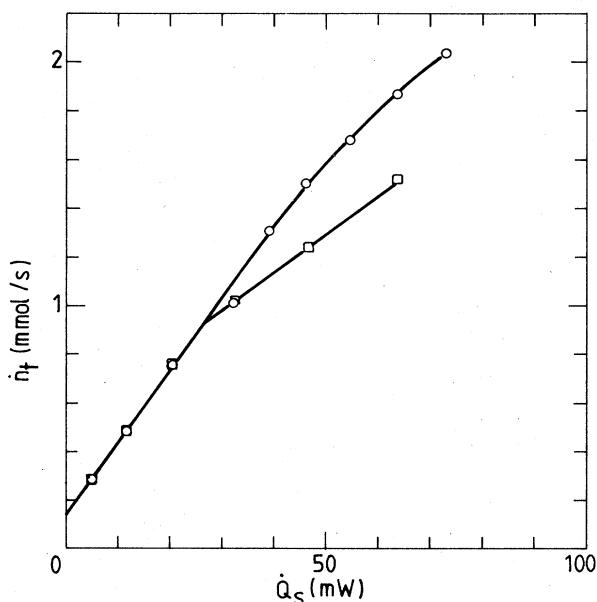


FIG. 3. Measured \dot{n}_t - \dot{Q}_s dependences with (○) and without (□) a superleak S parallel to the dilute side of the heat exchangers. In both cases $Z_m=0$.

machine to values larger than 0.92 mmol/s, all experiments described below were performed with $S||H$. In this case an appreciable amount of ^4He was circulated when $\dot{n}_t > 1.5$ mmol/s, due to the temperature rise in the still. If $\dot{n}_t < 1.5$ mmol/s, then $\dot{n}_t = \dot{n}_3$ within 6%.

The \dot{n}_t - \dot{Q}_s characteristics, measured with a superleak parallel to the heat exchangers ($S||H$), are dependent on the flow resistances Z_m in the mixing chamber. This is shown in Fig. 4. For large flow resistances (large L , small D), a kink at a critical flow rate \dot{n}_{tc} was observed similar to the kink shown in Fig. 3. For small flow resistances the kink was less pronounced.

Special attention should be paid to the curves 1, 6, and 7: curve 1 corresponds to $Z_m=0$, curve 6 corresponds to a relatively large Z_m ($L=23$ mm, $D=0.8$ mm) without superleak shunt, and curve 7 to the same Z_m but with superleak shunt $S||Z$. Again, the addition of a superleak shunt led to a significant increase of \dot{n}_t .

For $\dot{n}_t \gg \dot{n}_{tc}$ large amounts of ^4He were circulated. The experiments performed in this situation showed that the flow properties of the ^3He component, as reported in this paper, were not very sensitive to ^4He -circulation rates up to 50%. In this paper only the results of experiments in which the ^4He circulation rate was less than 6% of the total circulation rate [$\dot{n}_t < \min(\dot{n}_{tc}, 1.5 \text{ mmol/s})$] will be presented.

2. Pressure differences

Measurements of the pressure difference $\Delta p = p_m - p_e$ were performed with and without a superleak S shunted across Z_m . Results with $S||Z$ are shown in Fig. 5, where the variation in the capacitance of the pressure gauge is plotted against the right-hand side of Eq. (17), using the

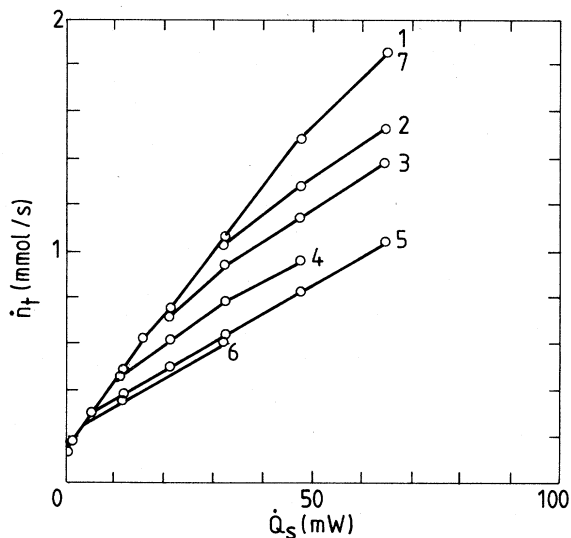


FIG. 4. Measured \dot{n}_t - \dot{Q}_s dependences with a superleak shunt across the heat exchangers ($S||H$) for different sizes of Z_m (L and D given in mm): 1, $Z_m=0$; 2, $L=23$, $D=1.6$; 3, $L=80$, $D=1.6$; 4, $L=700$, $D=1.6$; 5, $L=1400$, $D=1.6$; 6, $L=23$, $D=0.8$; and 7, $L=23$, $D=0.8$, with superleak shunt $S||Z$.

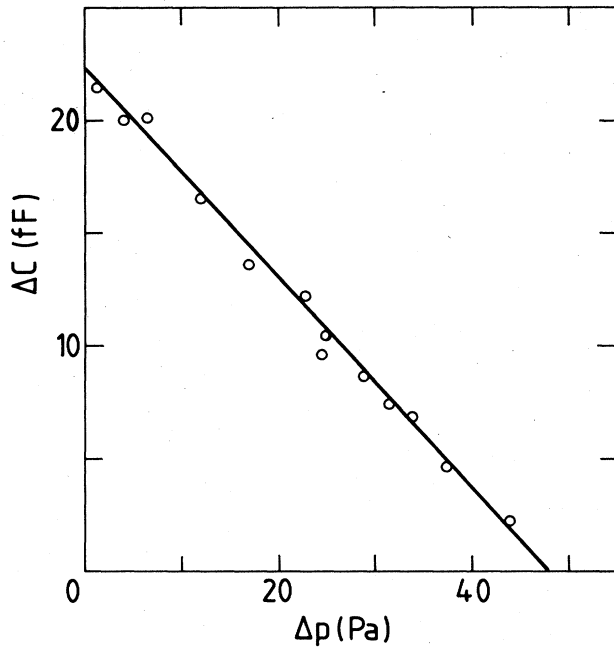


FIG. 5. Pressure changes across a tube shunted by a superleak ($S||Z$). The variation ΔC of the capacitance C of the pressure gauge (defined as $\Delta C = C - 2450$ fF) is plotted versus the pressure difference Δp calculated from the measured temperatures T_e and T_m with Eq. (17). The slope of the line is 460 ± 15 aF/Pa, in good agreement with the calibration of the pressure gauge (480 ± 30 aF/Pa).

measured temperatures T_e and T_m . The points show a linear relationship with a slope of 460 ± 15 aF/Pa, in agreement with the calibration of the pressure gauge of 480 ± 30 aF/Pa.

In the absence of a superleak, the pressure differences where on the order of magnitude of 1 Pa. This is 3 orders of magnitude smaller than the values of about 1000 Pa that would result from Eq. (17) and the measured $T_e^2 - T_m^2$ values, which were in this case much higher than with a superleak shunt. Pressure changes of 1 Pa are on the same level as the small variations due to circulating ^4He or due to hydrostatic effects. This leads to the important and simple flow property that, down to this level, the pressure difference due to the ^3He flow through ^4He II is zero:

$$p = \text{const} . \quad (23)$$

3. ^3He concentrations

The total change in ^3He concentration in Z_m is defined by

$$\Delta x = x_m - x_e . \quad (24)$$

The value of x_e was measured as described in Sec. IIB4. The value of x_m was obtained from T_m using the relation

$$x_m = 0.066 + 0.506T_m^2 - 0.249T_m^3 + 18.2T_m^4 - 74.2T_m^5 \quad (25)$$

for the concentration of the saturated dilute solution as a function of temperature.⁶ In Fig. 6 some typical results of $x_e - \dot{n}_t$ measurements are given. Curve 4 applies to the same Z_m as curve 6 in Fig. 4. In both curves a kink showed up at $\dot{n}_t = 0.3$ mmol/s. For $\dot{n}_t > 0.3$ mmol/s, x_e had a practically constant value of about 1.3%. Such a low x_e value led to a very low ^3He concentration in the liquid of the still, resulting in a high ^4He concentration in the vapor in the still (see Sec. IIC1). In Fig. 7 some typical $x_e - T_m$ dependences are given. To first order Δx is independent of T_m .

From double-logarithmic plots of Δx vs \dot{n}_t , as given in Fig. 8, it follows that

$$\Delta x = \beta \dot{n}_t^\alpha , \quad (26)$$

where α is a constant given by

$$\alpha = 2.8 \pm 0.4 , \quad (27)$$

independent of T_m , \dot{n}_t , L , or D . The parameter β depends on L and D , but not on T_m or \dot{n}_t .

Plots of \dot{n}_t vs D , at constant values of Δx , for flow impedances with length 23 mm,⁴ led to the relation

$$\dot{n}_t \sim D^2 . \quad (28)$$

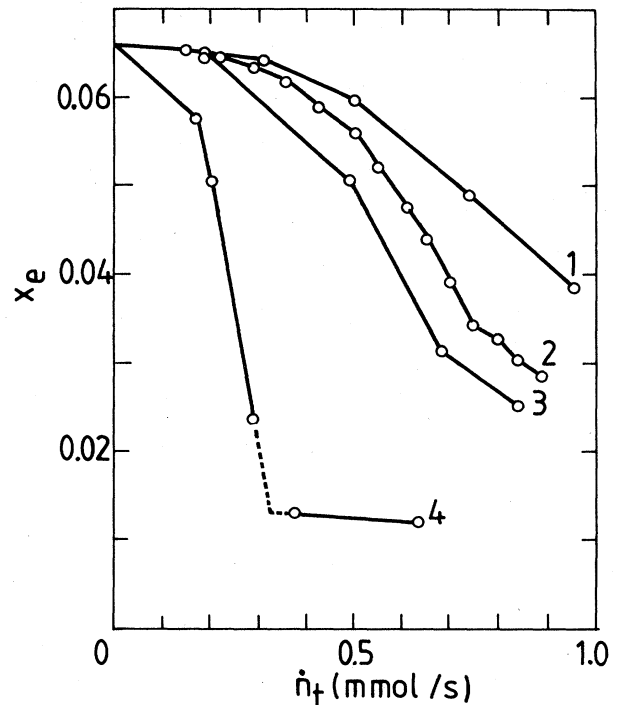


FIG. 6. Measured $x_e - \dot{n}_t$ dependences for $\dot{Q}_i = \dot{Q}_z = 0$ for four different sizes (mm) of Z_m : 1, $L=23$, $D=1.6$; 2, $L=10.5$, $D=1.2$; 3, $L=23$, $D=1.2$; and 4, $L=23$, $D=0.8$. The lines connecting the points are for visual aid only. The dotted part of curve 4 results from the extrapolation of the points with $\dot{n}_t < \dot{n}_{tc}$ and $\dot{n}_t > \dot{n}_{tc}$, respectively.

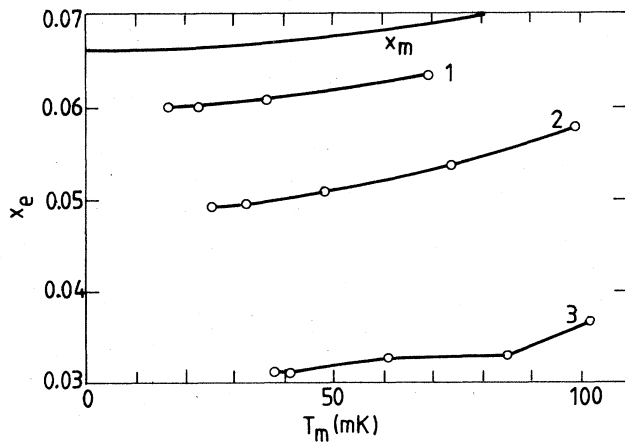


FIG. 7. Measured x_e - T_m dependences for $\dot{Q}_z=0$ for two sizes (mm) of Z_m and different values of \dot{n}_t (mmol/s): 1, $L=23$, $D=1.6$, $\dot{n}_t=0.51$; 2, $L=23$, $D=1.6$, $\dot{n}_t=0.76$; and 3, $L=23$, $D=1.2$, $\dot{n}_t=0.71$. The lines connecting the points are for visual aid only. The curve labeled x_m represents the x_m - T_m relationship calculated with Eq. (25).

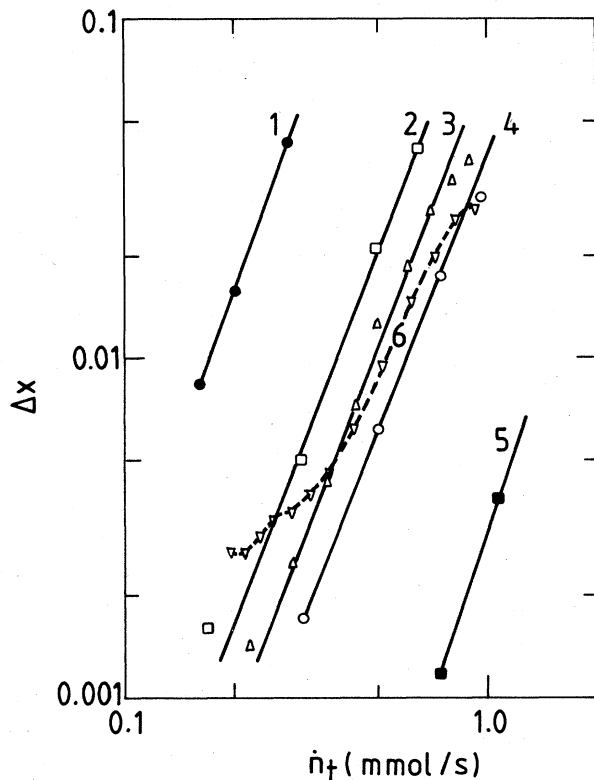


FIG. 8. Measured Δx - \dot{n}_t dependences for $\dot{Q}_i=\dot{Q}_z=0$ for the following tube sizes (mm): 1, $L=23$, $D=0.8$; 2, $L=130$, $D=1.6$; 3, $L=10.5$, $D=1.2$; 4, $L=23$, $D=1.6$; and 5, $L=23$, $D=2.3$. The straight lines represent Δx - \dot{n}_t dependences of the form $\Delta x \sim \dot{n}_t^\alpha$. The dotted curve 6 represents the Δx - \dot{n}_t relationship measured with the flow impedance as used by Wheatley and discussed in Sec. IV B.

Equation (28) suggests that the flow properties of the system are only dependent on the cross-sectional area of Z_m and not on the shape of the cross section. This would mean that the flow-rate density j_3 is homogeneous in the tube:

$$j_3 = \text{const.} \quad (29)$$

The validity of Eq. (29) was verified in an experiment in which Z_m consisted of four parallel tubes with $L=23$ mm and $D=0.6$ mm. The results turned out to be the same as with one single tube of the same length, with $D=1.2$ mm.

The concentration x as a function of l was measured with the setup depicted in Fig. 9. In this experiment, Z_m had a diameter of 1.6 mm and a total length of 130 mm. It was cut in four pieces with lengths of 8, 15, 37, and 70 mm, respectively. The pieces were connected by experimental spaces A , B , and C , in which x and T were measured.

In Fig. 10 the ^3He concentration x is plotted versus l for different \dot{n}_t . A linear x - l dependence was found. The

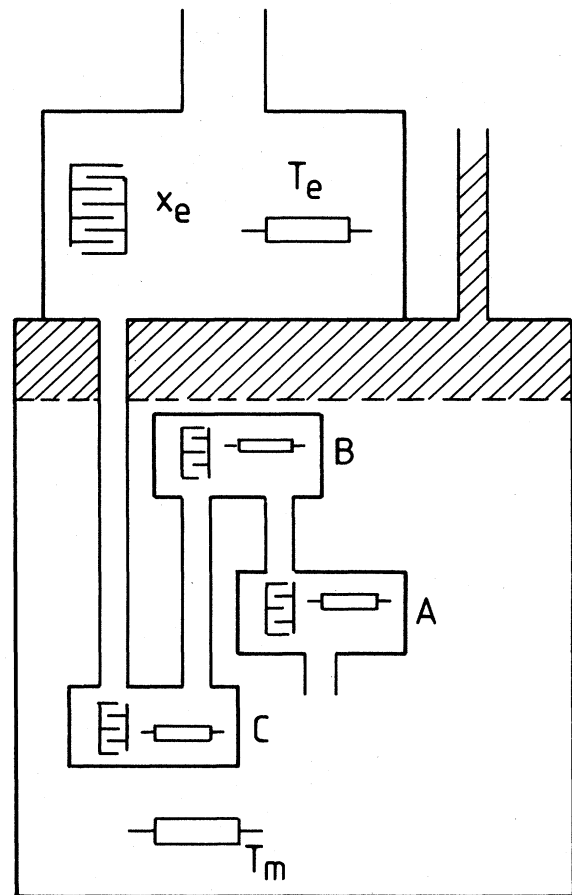


FIG. 9. Experimental setup for x - l measurements. In spaces A , B , and C , temperature and ^3He concentration were measured. The connecting tubes had equal diameters ($D=1.6$ mm). The lengths L were 8, 15, 37, and 70 mm, respectively.

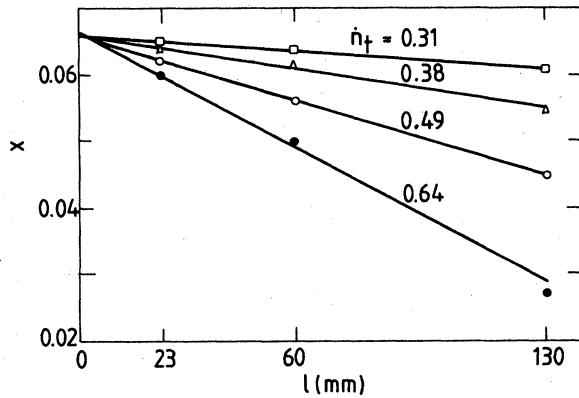


FIG. 10. Measured x - l dependences for four different flow rates indicated in the figure in mmol/s. The values of x and T were measured at $l=0, 23, 60,$ and 130 mm, respectively (see Fig. 9). The measured x - l dependences are represented by straight lines.

measured T^2 - l dependences were straight lines [Sec. II C 4, Eq. (35)]. Together with Eqs. (26) and (29), the x - l measurements lead to the equation

$$x = x_m - \gamma l j_3^\alpha \quad (30)$$

for the variation of the concentration along a tube. According to the experiments, γ is given by

$$\gamma = (35 \pm 3) \times 10^{-9} \text{ (SI units)}. \quad (31)$$

In calculating the value of γ in this paper, it is taken into account that \dot{n}_t contains on the average 3% ⁴He. This results in a 9% larger γ than the value reported in Ref. 4.

When $x_e=0$, then Eq. (30) leads to a maximum value j_c of j_3 given by

$$j_c = (x_m / \gamma L)^{1/\alpha}. \quad (32)$$

This critical ³He flow-rate density is responsible for the critical flow rate \dot{n}_{tc} which shows up in the \dot{n}_t - \dot{Q}_s curves as discussed in Sec. II C 1. It is an important quantity in the design of dilution refrigerators.¹⁶

4. Temperatures

The ³He enters the heat exchangers at the dilute side with a temperature T_e . The heat flow in the heat exchanger next to the mixing chamber is proportional to $T_i^4 - T_e^4$, so T_i is a function of T_e . When $T_e^4 \ll T_i^4$ the influence of T_e on T_i is small. However, when T_e is so large that it is comparable with T_i , an increase of T_e will also increase T_i because T_e always has to be smaller than T_i . In our machine, T_e satisfied the condition $T_e \leq 0.9T_i$. Since external heat leaks may be neglected in our case, it follows from the enthalpy balance of the mixing chamber in the low-temperature limit that $H_c T_i^2 = H_{3s}^* T_m^2$, which gives $T_i = 2.8T_m$. Hence, $T_e \leq 2.5T_m$. When $T_e \approx 2.5T_m$, the temperature increase in Z_m is nearly equal to the temperature decrease in the mixing chamber. In this paper this situation will be referred to as the "high-dissipation" limit.

The conservation of energy for a steady flow of ³He through ⁴He II can be formulated according to Eq. (1). In adiabatic flow, $\dot{Q}=0$ (see Sec. II B 2), hence,

$$H_3^* = \text{const}. \quad (33)$$

In our T - x region (10–150 mK, 2–7%) the enthalpy H_3^* is in good approximation a linear function of T^2 and x .⁶ Therefore, it is convenient to plot the experimental data in a T^2 - x diagram. In Fig. 11 the measured T_e^2 - x_e dependences are given for three different types of experiments.

In the *first* type \dot{n}_t was varied while $\dot{Q}_i=0$. When large flow resistances (and/or large flow rates) were used, the system was in the limit of high dissipation ($T_e \approx 0.9T_i$) as discussed above. In this case the T_e^2 - x_e relationship is represented by curve 4.

In the *second* type of experiments, \dot{n}_t was varied while T_m was fixed by adjusting \dot{Q}_i (in Fig. 11 curves 2 and 3, corresponding to $T_m=70$ and $T_m=40$ mK, respectively). The measured T_e^2 - x_e dependences can be represented by straight lines according to

$$T_e^2 + ax_e = T_m^2 + ax_m, \quad (34)$$

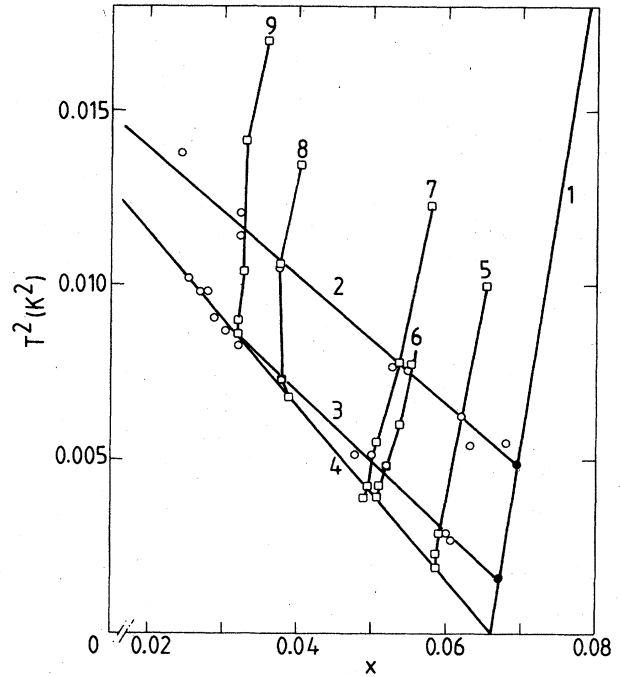


FIG. 11. T^2 - x diagram. Curves 1–9 mean the following: 1, Phase-separation line; 2, and 3, least-squares fit of measured T_e^2 - x_e points with constant values of $T_m=70$ and 40 mK, respectively. The T_m^2 - x_m points are indicated by \bullet . Points, indicated by \circ , represent T_e^2 - x_e measurements obtained with different flow rates and different Z_m ; 4, High-dissipation limit (also the limit of our experimental region in the T^2 - x diagram). With a dilution refrigerator only T_e^2 - x_e combinations can be achieved between curves 1 and 4; 5–9, T_e^2 - x_e dependences for constant \dot{n}_t and varying T_m . These points are represented by \square .

where a is an experimentally determined parameter which is independent of L , D , or \dot{n}_t . Its value varies slightly from 0.21 K^2 , at low temperatures, to 0.19 K^2 for $T_m = 70 \text{ mK}$. These values are in agreement with the calculated T^2 - x dependence of isenthalps [see Appendix, Eq. (A4)]. A relation for the temperature profiles can be found by combining Eqs. (30) and (34):

$$T^2 = T_m^2 + a\gamma l j_3^\alpha \quad (35)$$

At large flow rates the heating power \dot{Q}_i , necessary to fix T_m , was a decreasing function of \dot{n}_t . At a certain maximum flow rate \dot{Q}_i was zero. It was not possible to increase \dot{n}_t above this value without forcing T_m to rise. This is the limit of high dissipation as discussed above (curve 4).

A third set of curves (5–9) in the T^2 - x diagram was obtained by varying \dot{Q}_i for fixed \dot{n}_t . The T_e^2 - x_e curves are parallel to the phase-separation line, reflecting the observation that Δx is, to first order, constant for different T_m (compare Fig. 7). For $\dot{Q}_i = 0$, two situations can be distinguished:

(1) $T_e \ll 0.9T_i$. In this case the temperatures T_m , T_e , and T_i are determined by the performance of the heat exchangers.

(2) $T_e \approx 0.9T_i$. Again this is the high-dissipation limit. The points are situated on curve 4. In this case T_e is the minimum exit temperature ($T_{e,\min}$) for the given tube Z_m and with given \dot{n}_t . This temperature would be reached, even with zero thermal resistance in the heat exchangers, because it is determined by the dissipation in Z_m and not by the heat-exchanger performance. The corresponding minimum mixing-chamber temperature ($T_{m,\min}$) follows from

$$T_e \approx 0.9T_i = 2.5T_{m,\min} \quad (36)$$

5. Minimum mixing-chamber temperature

The minimum mixing-chamber temperature of a dilution refrigerator is a complicated function of the external heat load, the performance of the heat exchangers, and the exit-tube dimensions.¹⁶ The intrinsic low-temperature limit based on the MV model has been derived by Wheatley *et al.*³ At present it is not clear how this derivation has to be modified in order to take the mutual friction into account. A possibility has been sketched by de Waele *et al.*¹⁶

Here we will discuss the case in which the minimum temperature of the mixing chamber is determined by the temperature increase in Z_m [case (2) in Sec. IIC 4, Eq. (36)]. Combining Eqs. (35) and (36) leads to

$$T_{m,\min} = \frac{1}{2.3} (a\gamma L j_3^\alpha)^{1/2} \quad (37)$$

Some typical $T_{m,\min}$ - \dot{n}_t dependences calculated with Eq. (37) are drawn in Fig. 12. The asterisks marking the ends of the curves correspond to the critical flow-rate densities derived from Eq. (32). The experimental T_m - \dot{n}_t dependences with $\dot{Q}_i = \dot{Q}_z = 0$ are also given in Fig. 12. At low flow-rate values, T_m is determined by the heat exchangers

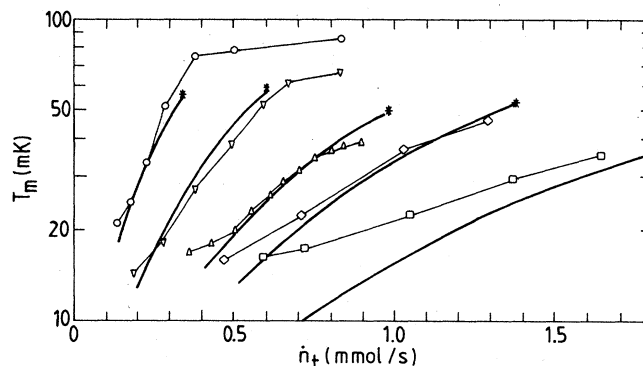


FIG. 12. Measured T_m vs \dot{n}_t for $\dot{Q}_i = \dot{Q}_z = 0$ for five different tubes (L and D in mm): $L=1382$, $D=1.6$ (\circ); $L=280$, $D=1.6$ (∇); $L=10.5$, $D=1.2$ (\triangle); $L=23$, $D=1.6$ (\diamond); and $L=5$, $D=1.6$ (\square). The solid curves are calculated with Eq. (37). Critical flow rates, corresponding with Eq. (32), are indicated with *. The lines connecting the measured points are for visual aid only.

[$T_e < 0.9T_i$, case (1) in Sec. IIC 4]. At high flow rates a high percentage of ^4He is circulated ($\dot{n}_t > \dot{n}_{t,c}$). At intermediate flow rates the measured T_m values are in agreement with Eq. (37).

6. Osmotic pressure

The osmotic pressure Π_e of the mixture in E was obtained from the measured x_e and T_e .⁶ In Fig. 13 a typical example is given. In this figure the Π_m - \dot{n}_t relationship is also given, where Π_m was obtained with the measured T_m ; x_m was calculated with Eq. (25). The line \triangle represents the osmotic pressure in the still, determined with the London device (Sec. IIB 5). The values of Π_s and Π_e are the same within the uncertainties of the calibration of the thermometer in the London device. Large

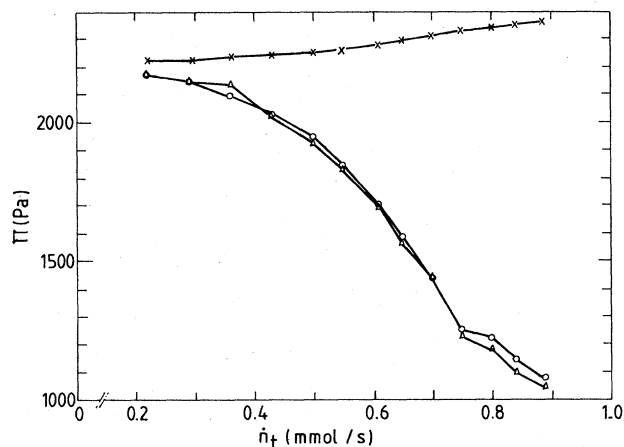


FIG. 13. Osmotic pressures in M , E , and in the still, plotted versus \dot{n}_t for a tube Z_m with $L=10.5 \text{ mm}$ and $D=1.2 \text{ mm}$. The osmotic pressures in M and E , represented by \times and \circ , respectively, are calculated from the measured x and T . The osmotic pressure in the still (\triangle) was determined with the London device.

differences between Π_e and Π_m were observed even though $\Delta p=0$ [compare Eq. (18)].

7. Nonadiabatic flow

In this subsection we will discuss experiments where a heating power \dot{Q}_z was supplied to the flowing ^3He . In the first set of experiments the ^3He was flowing through the heater with no flow resistance in series [$Z_m=0$, Fig. 14(a)]. Figure 15 is a T^2 - x diagram in which isotones (lines of constant osmotic pressure) are drawn,⁶ together with three pairs of T_e^2 - x_e , T_m^2 - x_m points. The osmotic pressures of the measured T_e^2 - x_e and the corresponding T_m^2 - x_m are equal. This demonstrates the important property that holds for $Z_m=0$: $\Pi_e=\Pi_m$ or $\mu_{4e}=\mu_{4m}$. These relations are the familiar relations for the steady state of ^3He flowing through ^4He in the absence of mutual friction.^{2,3}

In the second set of experiments, a flow resistance Z_m was connected in series with the heater in such a way that the ^3He , leaving M , first passed Z_m , passed next the heater, and then entered E [Fig. 14(b)]. The T_e^2 - x_e relationships were determined by varying \dot{Q}_z for a certain value of \dot{n}_t , while T_m was fixed within 1 mK by adjusting \dot{Q}_i . In Fig. 16 some typical results are given. The measured T_e^2 - x_e relationships for given T_m closely followed an isotone. This means that *not the ^3He concentration x_e , but the ^4He chemical potential μ_{4e} was constant.* The measurements with the London device also showed that Π_e was constant.

In the third set of experiments, the positions of Z_m and the heater were interchanged. Hence, the ^3He first passed the heater and then Z_m [Fig. 14(c)]. Again the T_e^2 - x_e relationships were measured for fixed T_m and \dot{n}_t . The T_e^2 - x_e dependences were the same as in the previous case. The pressure gauge between M and E showed that $\Delta p \approx 0$ as in the adiabatic flow experiments.

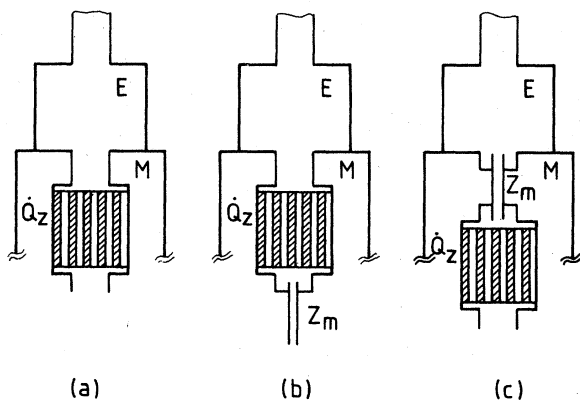


FIG. 14. Setups used in nonadiabatic flow measurements. (a) Heater connected between M and E without flow resistance in series. (b) Series connection of the flow impedance and the heater. ^3He first passes Z_m and then the heater. (c) Positions of Z_m and the heater are interchanged with respect to (b).

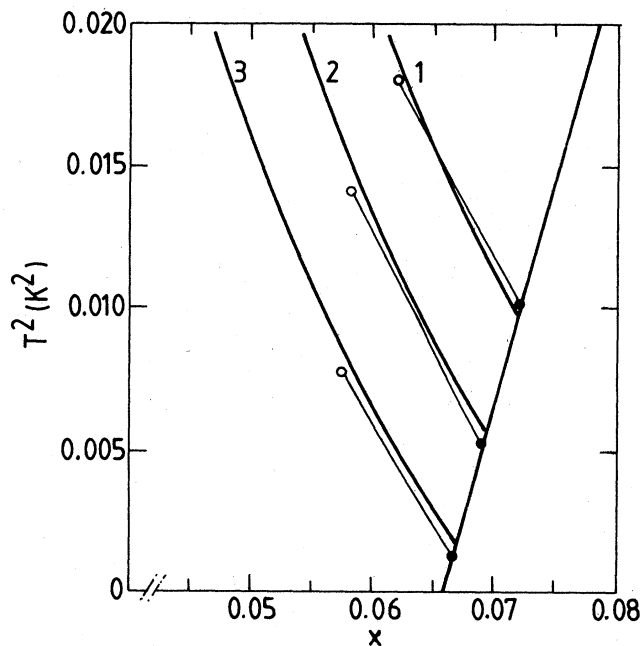


FIG. 15. Calculated lines of constant osmotic pressure: 1, $\Pi=3200$ Pa; 2, $\Pi=2800$ Pa; and 3, $\Pi=2400$ Pa. The points represent the measured T_e^2 - x_e (\circ) and corresponding T_m^2 - x_m (\bullet) in nonadiabatic flow measurements with $Z_m=0$ [Fig. 14(a)].

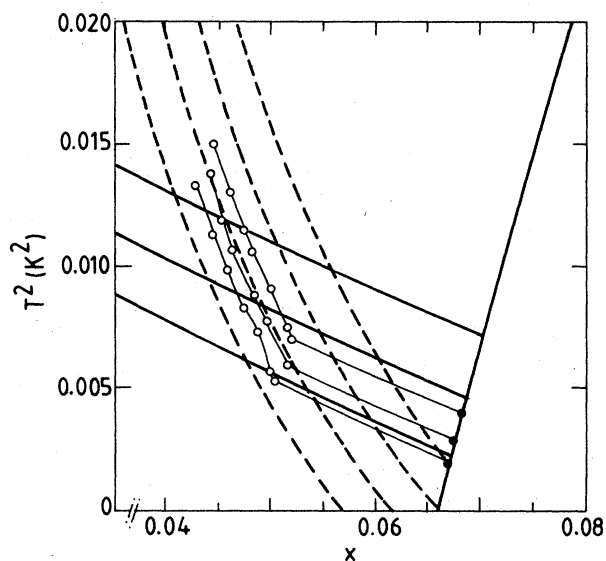


FIG. 16. Typical results of T_e^2 - x_e relationship in nonadiabatic flow experiment (\circ). The impedance Z_m ($L=23$ mm, $D=1.5$ mm) and the heater were connected in series according to Fig. 14(b). Measurements were performed with three different constant values of T_m (\bullet). The points were obtained by increasing \dot{Q}_z while adjusting \dot{Q}_i to fix T_m . The solid lines are isenthalps, the dashed lines represent isotones, and the thin lines connecting the points are for visual aid only. The flow rate was 0.75 mmol/s.

III. DOUBLE MIXING CHAMBER

A double mixing chamber (DMC) is a device in which the ^3He , circulating through a dilution refrigerator, is diluted in two steps.⁵ A schematic diagram is given in Fig. 17. A DMC can be installed in place of the single mixing chamber and can be used to extend the temperature range of a dilution refrigerator to lower temperatures. In the experiments described in this paper the DMC is used as a measuring device for the flow properties of ^3He - ^4He mixtures. Furthermore, a new explanation of the operation of the DMC will be given, based on the empirical relations obtained in Sec. II.

A. MV model

A full discussion of the DMC in the framework of the MV model is given by Coops *et al.*⁵ In this paper we give a simplified discussion: we neglect heat loads to the mixing chambers, we assume that all flow resistances in the DMC can be neglected, except the resistance of the dilute exit tube of the first mixing chamber Z_1 (diameter D , length L), and finally we assume that $\dot{n}_4 = 0$.

1. Temperature and flow distribution

The temperatures of the first and second mixing chamber (T_1 and T_2), and the dilute flow rate of the first mixing chamber (\dot{n}_1), can be obtained from \dot{n}_t , Z_1 , and the inlet temperature T_i , with the following relations:

$$\dot{n}_t H_c T_i^2 = \dot{n}_1 H_{3s}^* T_1^2 + (\dot{n}_t - \dot{n}_1) H_c T_1^2, \quad (38)$$

$$(\dot{n}_t - \dot{n}_1)(H_{3s}^* T_2^2 - H_c T_1^2) = 0, \quad (39)$$

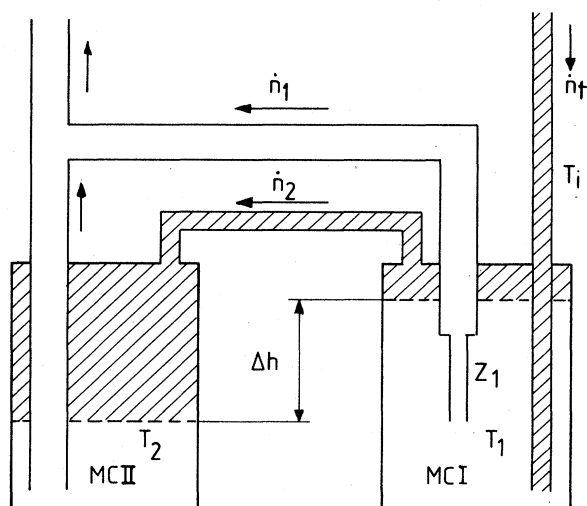


FIG. 17. Schematic drawing of a double mixing chamber. The hatched regions represent ^3He in the concentrated phase. The first and second mixing chamber are represented by MCI and MCII, respectively. Moles per second \dot{n}_1 (\dot{n}_2) of ^3He are diluted in MCI (MCII). The inlet temperature T_i could be varied with a heater at the entrance tube.

$$p_1 - p_2 = \frac{128L}{\pi D^4} \frac{\eta_0}{T_1^2} \dot{n}_1 V_3, \quad (40)$$

$$p_1 - p_2 = \Pi_s T_1^2 - \Pi_s T_2^2, \quad (41)$$

$$\Pi_s T_1^2 - \Pi_s T_2^2 = \frac{128L}{\pi D^4} \frac{\eta_0}{T_1^2} \dot{n}_1 V_3. \quad (42)$$

Equations (38) and (39) express enthalpy conservation for the first and second mixing chamber, respectively. Equation (40) follows from Eq. (8); Eq. (41) from Eq. (18). Equation (42) follows from Eqs. (40) and (41).

Equations (38)–(42) can be written in dimensionless form by introducing

$$t_1 = T_1/T_i, \quad t_2 = T_2/T_i, \quad r = \dot{n}_1/\dot{n}_t, \quad (43)$$

$$A_1 = \frac{H_{3s}^{*3}}{H_c^2(H_{3s}^* - H_c)} \frac{\eta_0 V_3}{\Pi_s} \frac{128L}{\pi D^4} \frac{\dot{n}_t}{T_i^4}, \quad (44)$$

resulting in

$$1 = \frac{H_{3s}^*}{H_c} r t_1^2 + (1-r)t_2^2, \quad (45)$$

$$(1-r) \left[\frac{H_{3s}^*}{H_c} t_2^2 - t_1^2 \right] = 0, \quad (46)$$

$$t_1^2 - t_2^2 = \frac{H_c^2(H_{3s}^* - H_c)}{H_{3s}^{*3}} \frac{A_1 r}{t_1^2}. \quad (47)$$

Equation (46) can be satisfied by $r=1$ or by $H_{3s}^* t_2^2 = H_c t_1^2$. From the analysis of Coops, it follows that

$$r = 1 \quad \text{for } A_1 \leq 1 \quad (48a)$$

and

$$H_{3s}^* t_2^2 = H_c t_1^2 \quad \text{for } A_1 \geq 1. \quad (48b)$$

If Eqs. (38)–(42) were valid, all measured t_1, t_2 - A_1 relationships would be independent of the individual values of L , D , \dot{n}_t , or T_i .

2. Level difference

The level difference Δh between the two phase boundaries follows from the condition for hydrostatic equilibrium:

$$\Delta \rho g \Delta h = p_1 - p_2, \quad (49)$$

where $\Delta \rho = 59 \text{ kg/m}^3$ is the difference between the densities of the dilute and the concentrated phases, respectively, and g is the gravitational acceleration. With Eqs. (41), (48), and (49), Δh can be expressed as a function of T_1 :

$$\Delta h = \frac{128L}{\pi D^4} \frac{\eta_0 V_3}{\Delta \rho g} \frac{\dot{n}_t}{T_1^2} \quad \text{for } A_1 \leq 1, \quad (50a)$$

$$\Delta h = \frac{H_{3s}^* - H_c}{H_{3s}^*} \frac{\Pi_s}{g \Delta \rho} T_1^2 \quad \text{for } A_1 \geq 1. \quad (50b)$$

With T_1 between 20 and 60 mK, values of Δh from 5 to 50 cm would result from Eqs. (50a) and (50b) for A_1 on the order of 2.

B. DMC with empirical relations of Sec. II

In this subsection we derive the properties of the DMC from Eqs. (25) and (30). According to Eq. (30), the ${}^3\text{He}$ flow rate \dot{n}_1 through Z_1 is determined by the concentration drop Δx across Z_1 . We assume that Δx is the result of the difference of T_1 and T_2 . For simplicity the slope of the T_m^2 - x_m dependence given by Eq. (25) will be approximated by a constant x_t which is, in the 40–150-mK region, equal to 0.6 K^{-2} within 15%. Hence,

$$\Delta x = x_1 - x_2 \approx x_t (T_1^2 - T_2^2). \quad (51)$$

1. Temperature distribution

Substituting Eq. (51) into (30) leads to

$$T_1^2 - T_2^2 = \frac{\gamma L}{x_t} \left[\frac{4\dot{n}_1}{\pi D^4} \right]^\alpha. \quad (52)$$

The relation is the analog of Eq. (42) derived from the MV model. It can be written in dimensionless form by introducing a parameter B defined by

$$B^\alpha = \frac{H_{3s}^{*2}}{H_c(H_{3s}^* - H_c)} \frac{\gamma L}{x_t} \left[\frac{4\dot{n}_t}{\pi D^2} \right]^\alpha \frac{1}{T_i^2}, \quad (53)$$

giving

$$t_1^2 - t_2^2 = \frac{H_c(H_{3s}^* - H_c)}{H_{3s}^{*2}} B^\alpha r^\alpha, \quad (54)$$

while

$$r = 1 \text{ for } B \leq 1 \quad (55a)$$

and

$$H_{3s}^* t_2^2 = H_c t_1^2 \text{ for } B \geq 1. \quad (55b)$$

The t_1, t_2 vs B relationships are similar to the t_1, t_2 vs A_1 relationships discussed in Sec. III B [Eq. (48a) and (48b)]. However, the definitions of the parameters A_1 and B are different, which implies a different relation between L , D , \dot{n}_t , and T_i .

2. Level difference

The experiments described in Sec. IIC 2 show that the pressure drop across Z_1 is zero [Eq. (23)]. Thus,

$$p_1 = p_2. \quad (56)$$

Hence, according to Eq. (49),

$$\Delta h = 0. \quad (57)$$

C. Experimental setup

The two mixing chambers were constructed from stainless-steel cylinders (inner diameter 30 mm; length 100 mm). The temperatures T_1 , T_2 , and T_i were measured in the liquid with calibrated resistance and CMN thermome-

ters. The inlet temperature T_i could be varied by supplying heat to the inlet tube (Sec. IIB 2). The total flow rate \dot{n}_t was varied with the heater in the still. The flow impedance Z_1 was usually installed at the entrance of the dilute exit channel of the first mixing chamber (see Fig. 17). The two mixing chambers were suspended at equal heights, within 0.1 mm.

The levels of the phase boundaries in the two mixing chambers were determined by capacitive level meters (Fig. 18) attached vertically to the tops of the mixing chambers. They consisted of two concentric metal cylinders with an axial slit in order to give the liquids free access to the annular region. The levels of the phase boundaries could be varied externally by varying the total amount of ${}^3\text{He}$ in the dilution refrigerator. The calibration was deduced from the capacitances, with the phase boundaries completely below and completely above the detectors, respectively. Level changes of $50 \mu\text{m}$ could be detected.

D. Experimental results

1. Temperature distribution

The temperatures T_1 and T_2 were measured as functions of \dot{n}_t and T_i for several different tube sizes. If a small flow resistance Z_1 was used (small L and large D), kinks in the T - \dot{n}_t relationships could be observed in our flow-rate region. In Figs. 19(a) and 19(b) the measured reduced temperatures, plotted versus A_1 and B , respective-

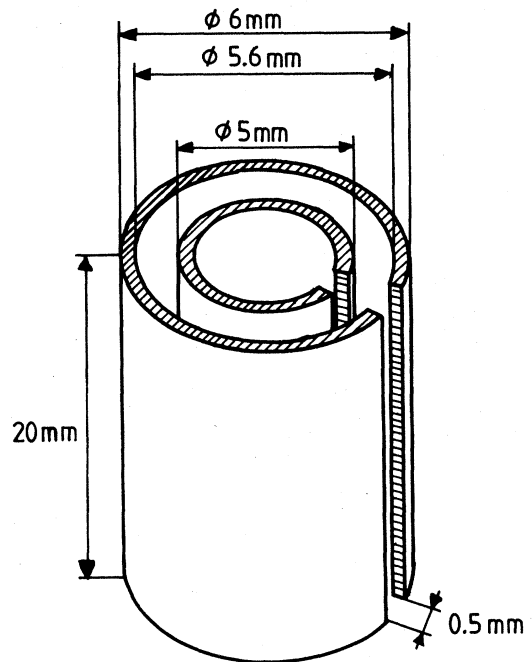


FIG. 18. Capacitor used for measuring the level of the phase boundary. The capacitance was about 10 pF. ϕ is a diameter.

ly, are given for a tube Z_1 with $L=5$ mm and $D=1.6$ mm.

The curves representing the experimental t_1, t_2 vs A_1 relationships show a dependence on \dot{n}_t . On the other hand, Fig. 19(b) shows that the reduced temperatures, plotted versus B , are independent of \dot{n}_t . The kink in the t_1-B and t_2-B curves is situated near $B=1.4$ instead of at $B=1$ [Eq. 55(a) and 55(b)]. This deviation may be due to the fact that the geometrical factor $L/D^{2\alpha}$ in B^α was modified because the length of this tube was not much larger than its diameter.

2. Level difference

The phase-boundary-level difference has been measured as a function of \dot{n}_t and T_1 for a number of different tube dimensions and double-mixing-chamber geometries. In general, tubes were chosen resulting in values of A_1 on the order of 2 in our T_1 region (Sec. III A 2). The measured Δh was usually on the order of 1 mm, much smaller than

values on the order of 10 cm calculated from Eq. (50). Sometimes Δh was even negative. The small measured values of Δh depended on the place where Z_1 was mounted in the DMC system.

The observed Δh values correspond to pressures of the order of 1 Pa. Similar to the situation discussed in Sec. IIC2, these pressure differences may be due to effects that were neglected in Eq. (56), such as variations in the densities of the liquids in the various parts of the DMC, the pressure drop in the concentrated connecting tube between the mixing chambers, or the ^4He in the circulating mixture.

For small flow resistances, kinks were observed in the $\Delta h-T_1$ dependences (cf. Sec. III D 1). This is demonstrated in Fig. 20, where the measured $\Delta h-T_1$ dependences for values of \dot{n}_t are given for the tube with $L=5$ mm and $D=1.6$ mm (cf. Fig. 19). In this figure the $\Delta h-T_1$ relationship, calculated with Eq. (50) for this tube with $\dot{n}_t=1$ mmol/s, is also presented.

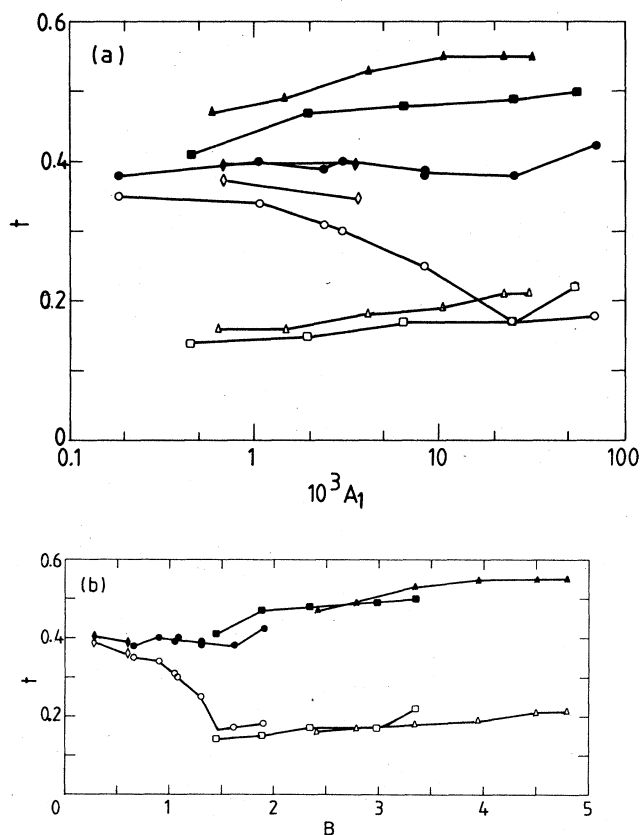


FIG. 19. Measured t_1 (solid symbols) and t_2 (open symbols) for a tube Z_1 with $L=5$ mm and $D=1.6$ mm. The value of T_1 was varied at four different flow rates [0.14 (\diamond); 0.48 (\circ); 1.03 (\square); 1.75 (\triangle) in mmol/s]. The results are plotted in two different ways: (a) As functions of parameter A_1 . $t-A_1$ dependences are dependent on the flow rate. (b) As functions of parameter B . $t-B$ dependences are not dependent on \dot{n}_t , in agreement with Eq. (54).

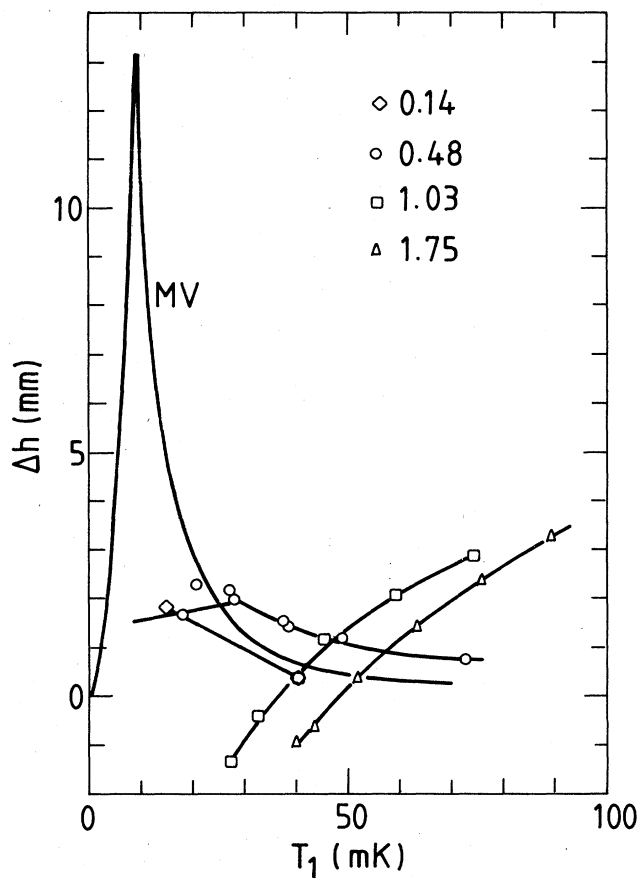


FIG. 20. Results of $\Delta h-T_1$ dependences measured with a tube Z_1 , with $L=5$ mm and $D=1.4$ mm (compare Fig. 19) for four different values of \dot{n}_t given in the inset. The lines connecting the points are for visual aid only. The curve labeled MV represents the $\Delta h-T_1$ dependence according to Eq. (50), calculated with $\dot{n}_t=1$ mmol/s. It should be compared with the squares in the figure. Measurements with other tubes showed that the $\Delta h-T_1$ dependences for T_1 values below the kink, were not dependent on the tube size.

IV. DISCUSSION

A. Mutual friction

The results of our experiments on the adiabatic flow properties of ³He moving through ⁴He, can be summarized by

$$p = \text{const} , \quad (23)$$

$$j_3 = \text{const} , \quad (29)$$

$$T^2 + ax = \text{const} , \quad (34)$$

and

$$x = x_m - \gamma' l j_3^\alpha . \quad (30)$$

The absence of any temperature dependence in Eq. (30) suggests that the ³He flow is completely determined by the concentration drop across the tube. However, due to the validity of Eq. (34), the difference of any linear combination of x and T^2 is proportional to j_3^α . From the experiments with nonadiabatic flow (Sec. IIC7) it can be seen that Δx changes when \dot{Q}_z changes, while the difference between the ⁴He chemical potentials in M and E is constant. Since μ_4 can be written as a linear combination of x and T^2 (see Appendix), Eq. (30) can be generalized to

$$\mu_4 = \mu_{4m} + \gamma' l j_3^\alpha , \quad (58)$$

where

$$\gamma' = 27 \times 10^{-9} \text{ (SI units)} . \quad (59)$$

The relations (23), (29), and (30) differ from the analogous relations (8), (9), and (20) obtained with the MV model. However, when $S||Z$ the experimental observations are in much better agreement with the predictions of the MV model. This can be explained by assuming a mutual friction between ³He and ⁴He:¹ without the superleak the motion of the ³He is impeded by the ⁴He. With $S||Z$ the ⁴He circulates between the mixing chamber, the tube, the experimental space, and the superleak. When in Z_m the ⁴He velocity is equal to the ³He velocity, the mutual friction force is zero there. Furthermore, the ⁴He chemical potential in the superleak is constant: $\mu_{4m} = \mu_{4e}$. Hence, the conditions for the MV model are satisfied.

B. Comparison with other work

In 1971, Wheatley *et al.*¹⁷ measured the temperature increase resulting from a flow impedance consisting of an annular space (width 0.1 mm) between two cylinders. The ³He was flowing perpendicular to the cylinder axis. The temperature range was 12 to 40 mK; the ³He flow rate varied between 10 and 53 $\mu\text{mol/s}$. Contrary to our observations, the experimental results were in good agreement with the MV model.

In order to investigate this discrepancy we duplicated the flow impedance used by Wheatley, carefully avoiding slits that might act as internal superleak shunts. Unfortunately, it was not possible to operate our refrigerator at flow rates below 150 $\mu\text{mol/s}$. In Fig. 8 the $\Delta x - \dot{n}_t$ measurements with $\dot{Q}_z = 0$ and $\dot{Q}_t = 0$ are represented by the dotted line. For $\dot{n}_t > 0.4$ mmol/s the $\Delta x - \dot{n}_t$ dependence is

almost the same as for a cylindrical tube with $L = 10.25$ mm and $D = 1.2$ mm, but for $\dot{n}_t < 0.4$ mmol/s, Δx tends to be larger. Furthermore, a dependence of Δx on T_m was found. The agreement with Eq. (26) was improved when T_m was increased, but there were still deviations from the \dot{n}_t^α behavior at lower flow rates.

Our measurements, extrapolated to low flow rates, did not agree with the MV model. On the other hand, we found deviations from the empirical relations, as determined with long cylindrical tubes. Apparently the geometry of the flow channel plays a role. A possible mechanism for geometry effects could be that in some cases macroscopic vortices of the total mixture develop inside the flow channel. Another reason for temperature-dependent deviations of the empirical relationships could be that there are slits in the system which act as superleaks. In this case the system will behave in accordance with the MV model.

Niinikoski¹⁸ reported the observation of large osmotic-pressure differences between the mixing chamber and the still (compare Sec. IIC6) which were not compensated by a fountain pressure or by a pressure drop due to the viscosity of the solution. From the flow impedance of Niinikoski's sintered heat exchangers, we estimate that the free passage in the heat exchangers is a slit with dimensions 7×0.4 mm². Using Eq. (32) with $x_m = 0.08$, a critical flow rate of 800 $\mu\text{mol/s}$ is found. This value is in the flow-rate range of 50–1200 $\mu\text{mol/s}$, as used by Niinikoski. According to our empirical relations, large deviations from the MV model should indeed be expected in this system.

Frossati¹⁹ observed anomalous $\dot{n}_3 - \dot{Q}_s$ behavior similar to the phenomena described in Sec. IIC1. In his experiment, a critical flow rate of about 60 $\mu\text{mol/s}$ was found with a tube in the dilute channel with $D = 0.5$ mm and an estimated length of 100 mm. From Eq. (32), a critical flow rate of 80 $\mu\text{mol/s}$ would follow. Furthermore, Frossati observed that with a tube with $D = 1.8$ mm and $L = 6$ m, flow rates up to 300 $\mu\text{mol/s}$ could be realized. This value should be compared with the critical flow rate of 240 $\mu\text{mol/s}$ following from Eq. (32).

In order to draw definite conclusions from the observations of Niinikoski and Frossati, more detailed information would be necessary. However, from the data available in Refs. 18 and 19, it seems justified to conclude that their observations are consistent with Eq. (32).

C. Hydrodynamic considerations

In this subsection the experimental observations are considered in the framework of the ³He-⁴He-II hydrodynamics. Some of the assumptions are rather speculative and need justification by a more detailed analysis in the future.

In the steady state the hydrodynamic equations of ³He-⁴He-II mixtures can be written as follows:

$$\nabla \cdot \rho_3 \mathbf{v}_3 = 0 , \quad (60)$$

$$\nabla \cdot \rho_4 \mathbf{v}_4 = 0 , \quad (61)$$

$$\nabla p = \eta (\Delta \mathbf{v}_3 + \frac{1}{3} \nabla (\nabla \cdot \mathbf{v}_3)) , \quad (62)$$

$$\nabla\mu_4 + V_4 F_{43} = 0, \quad (63)$$

where $\Delta = \nabla \cdot \nabla$, ρ_3 and ρ_4 are the densities of the ^3He and ^4He components, \mathbf{v}_3 and \mathbf{v}_4 their respective time-averaged velocities, and V_4 the volume of the mixture containing 1 mole of ^4He . The mutual-friction-force density between the ^3He and the ^4He is denoted by F_{43} . Terms of second and higher order in the velocities are neglected. Furthermore, we assume that the temperature is so low that the influence of the normal component of the ^4He II can be neglected.

We consider a flow through a long cylindrical tube and assume that the vectors \mathbf{v}_3 and \mathbf{v}_4 are in the direction of the tube axis and that μ_4 and p are constant in a plane perpendicular to the axis. Equation (63) gives

$$\frac{d\mu_4}{dl} + V_4 F_{43} = 0, \quad (64)$$

where F_{43} represents the magnitude of the vector \mathbf{F}_{43} . A similar notation will be used for the other vectors.

In pure ^4He II, the Gorter-Mellink mutual-friction-force density \mathbf{F}_{sn} between the superfluid and normal components is given by²⁰

$$\mathbf{F}_{sn} = A\rho_s\rho_n |\mathbf{v}_s - \mathbf{v}_n|^2 (\mathbf{v}_s - \mathbf{v}_n), \quad (65)$$

where ρ_s and ρ_n are the superfluid and normal densities and A is the Gorter-Mellink parameter (which is of the order of magnitude of 500 sm/kg). In analogy, we assume that F_{43} can be written in the form

$$F_{43} = A_{43}\rho_3\rho_4 |v_4 - v_3|^{q-1} (v_4 - v_3) \quad (66)$$

or

$$v_3 = v_4 + \left[\frac{-F_{43}}{A_{43}\rho_3\rho_4} \right]^{1/q}, \quad (67)$$

where q is a constant. With Eq. (64) the relative velocity

$$v_{43} = v_3 - v_4 \quad (68)$$

is given by

$$v_{43} = \left[\frac{d\mu_4/dl}{A_{43}\rho_3 M_4} \right]^{1/q} \quad (69)$$

In Eq. (69) M_4 is the molar mass of the ^4He . Since μ_4 is constant in a plane perpendicular to the tube axis, v_{43} is also constant in this plane. In particular,

$$v_{4w} = v_{3w} - v_{43}, \quad (70)$$

where v_{3w} and v_{4w} are the velocities of the ^3He and ^4He near the wall.

Since $L \gg D$, the second derivative of the velocity in the axial direction is usually much smaller than in the radial direction. If we neglect the contribution of the axial term, Eq. (62) leads to the well-known relation

$$v_3 = v_{3w} + (r^2 - \frac{1}{4}D^2) \frac{dp/dl}{4\eta}. \quad (71)$$

This gives for the total ^3He flow rate through the tube,

$$V_3 \dot{n}_3 = \frac{1}{4} \pi D^2 v_{3w} - \frac{\pi D^4}{128\eta} \frac{dp}{dl}. \quad (72)$$

The ^4He flow rate satisfies

$$V_4 \dot{n}_4 = V_3 \dot{n}_3 - \frac{1}{4} \pi D^2 v_{43}. \quad (73)$$

With Eqs. (70) and (72) follows

$$V_4 \dot{n}_4 = \frac{1}{4} \pi D^2 v_{4w} - \frac{\pi D^4}{128\eta} \frac{dp}{dl}. \quad (74)$$

In our experiments, \dot{n}_3 and \dot{n}_4 are imposed externally. The ^4He flow rate is in good approximation equal to zero:

$$\dot{n}_4 = 0. \quad (75)$$

In the MV model it is assumed that $v_{3w} = 0$, similar to the case of a flowing single-component viscous fluid. However, in the case of a combined diffusive and viscous flow,²¹ it is a linear combination of the velocities of the two components that is assumed to be zero at the walls. In analogy, we write for the boundary condition,

$$\rho_3 v_{3w} + f_w \rho_4 v_{4w} = 0, \quad (76)$$

where f_w is a dimensionless parameter that accounts for the difference in strengths of the forces between the wall and each of the two components, respectively. Good agreement with our experiments can be obtained if a strong frictional force between the ^4He and the boundary is assumed, such that $f_w \gg 1$. It then follows that $v_{4w} \ll v_{3w}$. As a first approximation we take

$$v_{4w} = 0. \quad (77)$$

Substitution in Eq. (70) gives

$$v_{3w} = v_{43}, \quad (78)$$

and from Eqs. (74)–(77) follows

$$\frac{dp}{dl} = 0. \quad (79)$$

In our model, the momentum transfer of the ^3He to the wall is compensated by an infinitesimally small ^4He flow which sticks strongly to the wall. This is an explanation of the remarkable properties, that the pressure is constant in the tube and that the ^3He velocity is nonzero near the wall.

The zero-pressure gradient leads to a flat velocity profile for both components:

$$v_3 = v_{3w}, \quad (80)$$

$$v_4 = 0. \quad (81)$$

Furthermore, it follows from Eq. (69) that

$$\frac{d\mu_4}{dl} = A_{43}\rho_3 M_4 V_3^q \left[\frac{\dot{n}_3}{\frac{1}{4} \pi D^2} \right]^q \quad (82)$$

or

$$\frac{d\mu_4}{dl} = \gamma'' j_3^q, \quad (83)$$

with

$$\gamma'' = A_{43} M_3 M_4 V_3^{q-1}. \quad (84)$$

M_3 is the ³He molar mass.

Here, equations (79)–(82) have been derived for cylindrical tubes. It is also possible to derive these expressions for the more general case of a long tube with a constant cross section of arbitrary shape. In that case one can use Green's theorem to derive that $v_4=0$ everywhere in the tube from the assumption that $v_{4w}=0$. The relations (79)–(84) are consistent with experiments if

$$q = \alpha \quad (85)$$

and

$$\gamma'' = \gamma' \quad (86)$$

Within experimental accuracy, the value of q is equal to the exponent in the Gorter-Mellink force [Eq. (65)]. The value of A_{43} , calculated with Eqs.(84)–(86) for a 6.6% mixture, is strongly dependent on the value of α . With a variation of α from 2.4 to 3.2, the value of A_{43} varies from 100 to 60 000. With $\alpha=2.8$, the value of A_{43} would be 2600 sm/kg; a value of $A_{43}=A=500$ sm/kg would give $\alpha=2.6$.

The mathematical expressions for the mutual-friction-force densities are the same. In addition, $q=\alpha$ and $A_{43}=A$ within experimental accuracy. This strongly suggests that the mechanisms responsible for the mutual friction between normal and superfluid ⁴He, and between ³He and ⁴He, are the same. In pure ⁴He II the mutual friction is caused by a ⁴He vortex tangle.²² It is conceivable that the motion of the ³He generates a ⁴He vortex tangle in a similar way.

This suggestion is supported by experiments of Awaschalom *et al.*,²³ who found that v_n is homogeneous in ⁴He II, just as is v_3 in our experiments, and by experiments by Baehr and Tough,²⁴ who showed that the wall plays an important role in the ⁴He II hydrodynamics. The presence of a ⁴He vortex tangle may justify our assumption that the ⁴He is strongly clamped to the walls.

The ³He flow properties can provide a powerful tool to investigate the ⁴He tangle: contrary to the situation in pure ⁴He II, the temperature and the normal-component fraction can be varied independently. Since ³He has a nuclear spin, NMR techniques can be used.²⁵ Furthermore, the fact that the ³He cannot be converted into ⁴He, may simplify the description of the flow properties. The fundamental aspects of the flow properties of ³He-⁴He mixtures are presently under theoretical and experimental investigation in our group.

ACKNOWLEDGMENTS

We wish to thank all the students that contributed to our research, but especially H. P. L. Levels, J. C. M. Keltjens, and H. W. M. P. Keusters. We thank L. C. van Hout and L. M. W. Penders for their technical support, and J. J. G. M. van Amelsvoort and W. C. T. H. Delissen for the liquid-helium supply. Professor Dr. W. van Haeringen and Professor Dr. J. T. L. Devreese are acknowledged for their stimulating interest in our work.

APPENDIX: LOW-TEMPERATURE LIMITING VALUES OF SOME LIQUID PROPERTIES

In this appendix we shall give the low-temperature limiting values of some properties of pure ³He and of ³He-⁴He mixtures for concentrations near saturation ($x \approx x_0$). For thermodynamic quantities that are to first order proportional to T^2 , we write the approximation in the form

$$F(T, x) = F(0, x_0) + F_x(x - x_0) + F_T T^2, \quad (A1)$$

where F_x and F_T are constants. In Eq. (A1) the symbol F stands for H_3^* , Π , μ_3 , or μ_4 . The values of $F(0, x_0)$, F_x , and F_T are obtained from Kuerten *et al.*⁶ and are listed in Table I.

The dilute side of the phase-separation curve is given by

$$x_s(T) = x_0 + 0.506 T^2. \quad (A2)$$

With Eqs. (A1) and (A2), one can calculate the values of the thermodynamic quantities on the phase-separation curve. In general,

$$F(T, x_s(T)) = F(0, x_0) + F_s T^2. \quad (A3)$$

The values of F_s are also given in Table I. The T^2 - x dependence at constant H_3^* is given by

$$T^2 + a'x = \text{const} \quad \text{with} \quad a' = H_{3x}^*/H_{3T}^* = 0.209 \text{ K}^2. \quad (A4)$$

The specific heat C_{3d} and the entropy S_F per mole ³He of the dilute mixture with $x = x_0$ are given by

$$C_{3d} = S_F = C_0 T \quad \text{with} \quad C_0 = 104 \text{ J/mol K}^2. \quad (A5)$$

The viscosity of the mixture is given by⁸

$$\eta = \eta_0 / T^2 \quad \text{with} \quad \eta_0 = 5 \times 10^{-8} \text{ s Pa K}^2. \quad (A6)$$

The thermal conductivity of the mixture satisfies²⁶

$$\kappa = \kappa_0 / T \quad \text{with} \quad \kappa_0 = 3 \times 10^{-4} \text{ W/m}. \quad (A7)$$

The volume per mole ³He is

TABLE I. Values of $F(0, x_0)$, F_x , F_T , and F_s for some thermodynamic quantities.

F	$F(0, x_0)$	F_x	F_T	F_s
x	0.066	1	0	0.506 K^{-2}
H_3^*	0 J/mol	17.58 J/mol	84.06 J/mol K ²	92.95 J/mol K ²
Π	2209 Pa	45.0 kPa	81.7 kPa/K ²	104.4 kPa/K ²
μ_3	0 J/mol	17.58 J/mol	-20.28 J/mol K ²	-11.39 J/mol K ²
μ_4	-0.06092 J/mol	-1.242 J/mol	-2.253 J/mol K ²	-2.882 J/mol K ²

$$V_3 = V_4^0(1 + 0.286x)/x \quad \text{with } V_4^0 = 27.58 \times 10^{-6} \text{ m}^3. \quad (\text{A8})$$

The constant b , determining the slope of the T^2 - x dependence in the case of viscous, adiabatic flow, Eq. (19), is given by

$$b = \frac{\Pi_x}{\Pi_T + \frac{1}{2}C_0/V_3} = 0.217 \text{ K}^2. \quad (\text{A9})$$

The low-temperature limit of the enthalpy H_3^0 of pure ^3He is given by²⁷

$$H_3^0 = H_c T^2 \quad \text{with } H_c = 11.4 \text{ J/mol K}^2; \quad (\text{A10})$$

the specific heat C_3^0 and the entropy S_3^0 by

$$C_3^0 = S_3^0 = C_c T \quad \text{with } C_c = 22.8 \text{ J/mol K}. \quad (\text{A11})$$

-
- ¹G. M. Coops, A. T. A. M. de Waele, and H. M. Gijsman, *Phys. Rev. B* **25**, 4879 (1982).
- ²J. C. Wheatley, *Am. J. Phys.* **36**, 181 (1968).
- ³J. C. Wheatley, O. E. Vilches, and W. R. Abel, *Ann. Physics (N.Y.)* **4**, 1 (1968).
- ⁴A. T. A. M. de Waele, J. C. M. Keltjens, C. A. M. Castelijns, and H. M. Gijsman, *Phys. Rev. B* **28**, 5350 (1983).
- ⁵G. M. Coops, A. T. A. M. de Waele, and H. M. Gijsman, *Cryogenics* **19**, 659 (1979).
- ⁶J. G. M. Kuerten, C. A. M. Castelijns, A. T. A. M. de Waele, and H. M. Gijsman, *Physica* **128B**, 197 (1985).
- ⁷W. van Haeringen, *Cryogenics* **20**, 153 (1980).
- ⁸K. A. Kuenhold, D. B. Crum, and R. E. Sarwinski, *Phys. Lett.* **41A**, 13 (1972).
- ⁹A. T. A. M. de Waele, A. B. Reekers, and H. M. Gijsman, in *Quantum Fluids and Solids*, edited by S. B. Trickey, E. D. Adams, and J. W. Dufty (Plenum, New York, 1977), p. 451.
- ¹⁰P. Das, R. de Bruyn Ouboter, and K. W. Taconis, in *Proceedings of the IXth International Conference on Low Temperature Physics, Columbus, Ohio, 1964*, edited by J. G. Daunt, D. O. Edwards, F. J. Milford, and M. Yagub (Plenum, New York, 1965), p. 1253.
- ¹¹A. T. A. M. de Waele, G. M. Coops, T. Satoh, and H. M. Gijsman, in *Proceedings of the Eighth International Cryogenic Engineering Conference, Geneva, 1980*, edited by C. Rizzuto (IPC Science and Technology, Guildford, England, 1980), p. 451.
- ¹²J. F. Schooley, G. A. Evans, Jr., and R. J. Soulen, Jr., *Cryogenics* **20**, 193 (1980).
- ¹³H. A. Kierstead, *J. Low Temp. Phys.* **24**, 497 (1976).
- ¹⁴H. London, H. Berks, D. Phillips, and G. P. Thomas, in *Proceedings of the Eleventh International Conference on Low Temperature Physics, St. Andrews, 1968*, edited by J. F. Allen, D. M. Finlayson, and D. M. McCall (St. Andrews, 1968), p. 649.
- ¹⁵A. T. A. M. de Waele, G. J. van der Geest, H. P. L. Levels, and H. M. Gijsman, in *Proceedings of the Ninth International Cryogenic Engineering Conference, Kobe, Japan 1982*, edited by Yasukochi and Nagano (Butterworth, Guildford, England, 1982), p. 625.
- ¹⁶A. T. A. M. de Waele, J. C. M. Keltjens, C. A. M. Castelijns, and H. M. Gijsman, in *Advances in Cryogenic Engineering*, edited by R. W. Fast (Plenum, New York, 1984), Vol. 29, p. 565.
- ¹⁷J. C. Wheatley, R. E. Rapp, and R. T. Johnson, *J. Low Temp. Phys.* **4**, 1 (1971).
- ¹⁸T. O. Niinikoski, *Nucl. Instrum. Methods* **97**, 95 (1971).
- ¹⁹G. Frossati, H. Godfrin, B. Hebral, G. Schumacher, and D. Thoulouze, in *Physics at Ultralow Temperatures, Proceedings of the International Symposium at Hakone*, edited by P. Sugawara (Physical Society of Japan, Tokyo, 1977), p. 205.
- ²⁰C. J. Gorter and J. H. Mellink, *Physica* **15**, 285 (1949).
- ²¹L. Waldmann and K. H. Schmitt, *Z. Naturforsch., Teil A* **16**, 1343 (1961).
- ²²J. T. Tough, in *Progress in Low Temperature Physics VIII*, edited by D. F. Brewer (North-Holland, Amsterdam, 1982), p. 133, and the references therein.
- ²³D. D. Awschalom, F. P. Milliken, and K. W. Schwarz, *Phys. Rev. Lett.* **53**, 1372 (1984).
- ²⁴M. L. Baehr and J. T. Tough, *Phys. Rev. Lett.* **53**, 1669 (1984).
- ²⁵M. Okuyama, T. Satoh, T. Satoh, T. Ohtsuka, T. Sato, and S. Saito, in *Proceedings of the 17th International Conference on Low Temperature Physics, Karlsruhe, FRG, 1984*, edited by U. Eckern, A. Schmid, W. Weber, and H. Wuhl (North-Holland, Amsterdam, 1984), p. 303.
- ²⁶W. R. Abel and J. C. Wheatley, *Phys. Rev. Lett.* **21**, 1231 (1968).
- ²⁷D. S. Greywall, *Phys. Rev. B* **27**, 2747 (1983).